Poly (Ethylene Terephthalate) Oligomers Cationized by Alkali Ions: Structures, Energetics, and Their Effect on Mass Spectra and the Matrix-Assisted Laser Desorption/Ionization Process

Jennifer Gidden, Thomas Wyttenbach, Joseph J. Batka, and Patrick Weis
Department of Chemistry, University of California, Santa Barbara, California, USA

Anthony T. Jackson and James H. Scrivens
ICI Research and Technology Centre, Wilton, Middlesbrough Cleveland, UK

Michael T. Bowers
Department of Chemistry, University of California, Santa Barbara, California, USA

In this article the folding dynamics and energetics for a set of poly(ethylene terephthalate) (PET) oligomers cationized by various alkali ions are studied: M^+PETn for $n = 2$ to 7 and M = Li, Na, and K. Experimental cross sections were determined for matrix-assisted laser desorption/ionization (MALDI) generated ions using the ion mobility based ion chromatography method. Very good agreement was obtained with cross sections generated by the AMBER 4.0 suite of molecular dynamics programs. For $n = 2$ and 4 the benzene rings of the oligomers π stack with the metal ion coordinated to both terminal hydroxyl oxygen atoms and several of the nearby carbonyl oxygen atoms. For $n = 3$, two isomers are both observed and predicted by theory: an open form where the third PET monomer attaches to the dimer and extends into space and a closed form where the third PET moiety bends back and coordinates its hydroxyl oxygen with the metal ion. For Na^+PET3, equilibrium is observed between 100 and 180 K with an Arrhenius analysis yielding an open to closed form isomerization barrier of 1.6 kcal/mol. For this same system the two isomeric forms are frozen out at 80 K and coupling the observed isomeric distribution with an RRKM analysis indicates the closed form is more stable by 0.5 kcal/mol. For K^+PET3 the barrier to isomerization is too low to observe (<1.0 kcal/mol), whereas for Li^+PET3 a temperature independent isomer distribution is observed (80 to 55°K). Using methods developed for determining isomerization barriers in carbon clusters it was possible to obtain an open to closed form isomerization barrier of 7 ± 2 kcal/mol for Li^+PET3. In this system, the open and closed form isomer populations were observed to be strong functions of the laser power in the MALDI source. This allowed a detailed description of the formation mechanism to be formulated and indicated alkali ion attachment to the polymer during expansion of the plume emanating from the surface. Finally, the mass spectrum of a PET oligomer sample has been shown to strongly depend on the cationizing alkali metal ion. It is qualitatively shown that M^+–PETn binding energies and structures are responsible. (J Am Soc Mass Spectrom 1999, 10, 883–895) © 1999 American Society for Mass Spectrometry

Considerable attention has been paid to the structures of macromolecules and their complexes because of the strong influence of structure on observed properties. For example, the arrangement of base pairs in DNA controls protein synthesis and gene replication [1]. The size and shape of the ring cavity in crown ethers affect metal ion selectivity [2]. Enzymes fit particular substrates, and antibodies have specific forms that recognize specific diseases [3].

Although most of the work in this area focuses on biopolymers, relatively few gas phase studies have examined the structure-function relationship in synthetic polymers. Many properties of synthetic polymers, such as chemical and thermal stability, various transition temperatures, and the ability to be molded and spun, depend on the polymer's molecular structure [4].

Address reprint requests to Michael T. Bowers, Department of Chemistry, University of California, Santa Barbara, CA 93106.

Dedicated to the memory of Professor Robert Squires.

1044-0305/99/$20.00
PII S1044-0305(99)00054-9

Received February 15, 1999
Revised April 19, 1999
Accepted April 19, 1999

This "structure" can be characterized several ways. It can be described by an average molecular weight or molecular weight distribution, by the chemical composition of the monomer units and end groups, by the monomer sequence in copolymers, or by the relative spatial arrangement of the polymer atoms. It is this latter aspect that will interest us here.

One method that is developing into a promising tool for probing the structures of polymers is mass spectrometry. With the aid of matrix-assisted laser desorption/ionization (MALDI) [5] these large molecules can be transferred to the gas phase with little or no fragmentation. MALDI-MS has been used to accurately measure molecular weight distributions of a wide range of polymers [6–9]. It has also been used to determine the chemical nature of the repeat units and end groups via the resolution of individual oligomers and collision induced dissociation analyses [10–12]. MALDI-MS studies have even examined how the cationizing agent influences the characterization of polymers [13–15]. The molecular weight distributions of poly(methyl methacrylate) (PMMA) [14] and poly(ethylene terephthalate) (PET) [15] changed significantly when different alkali ions were added. The change was attributed to less favorable interactions between large cations and small oligomers thus creating an apparent shift in the distribution.

Our interests focus more on the actual geometrical shape of the polymer and how this shape varies with the size of the polymer and nature of the cationizing agent. Surprisingly, little is known about the conformations of this fundamentally and industrially significant class of molecules. Although polymers can have a large number of different conformations due to easy rotations about single bonds, relatively few of them are energetically favorable. Therefore, it is important to identify these preferred conformations of polymers and examine the factors that control the dynamics of changing conformations.

Our group utilizes a technique that combines mass spectrometry with ion mobility methods in what we term "ion chromatography" (IC) [16] to obtain detailed structural information on large molecular ions. IC essentially separates, in time, ions with different geometric shapes. These different shaped ions have different collision cross sections and, as a result, have different mobilities when drifting through a buffer gas under the influence of a weak electric field. Various computational methods are then used to generate proposed structures of the ions and calculate their cross sections to compare with those obtained from the IC experiments. This combination has been successfully used to distinguish between different geometrical isomers of carbon clusters and determine how the structure changed as a function of size [17]. It has also been applied to various sized biopolymers [18–23] as well as synthetic polymers [24–27]. For poly(ethylene glycol) (PEG) [25, 26] it was found that the flexible PEG oligomers completely encapsulated the cationizing metal ion (coordinating up to 11 oxygen centers for Cs^+), forming a nearly spherical shape. Slightly less flexible poly(methyl methacrylate) oligomers, however, are cyclic with the metal ion primarily coordinating to the oxygen atoms on the ends of the oligomer [27]. By contrast, polystyrene forms open chains with the benzene rings π stacking and the metal ion sandwiched between two of them [28]. Significant effort was put into all of these systems to develop a general protocol for using IC on large molecules and to determine the parametrization required to accurately measure the conformations of these molecules.

In order to further test our IC method, to begin to answer some questions about the conformations, energetics, and dynamics of synthetic polymers, and to address issues raised in the cation dependence of the oligomer distribution [15], we extended our studies to PET, one of the most widely used polyesters in industry. This is a particularly interesting polymer because it has both flexible and stiff segments that may lead to rather elaborate structures and folding dynamics. In this paper we will discuss PET oligomers for $n = 2–7$ and use the symbol M^+PETn to represent these oligomers capped by OH and CH_2CH_2OH groups as shown above and cationized by the alkali ion M. In addition to obtaining the actual PET structures, we are also interested in determining the relative energies of the various conformations, examining the energetics and dynamics of converting from one conformer to another, and establishing relative binding energies of the different alkali ions as a function of oligomer size. We will use this information to address practical issues associated with the MALDI process and with the use of MALDI-TOF (or other instruments) to accurately measure oligomer distributions and average molecular weights.

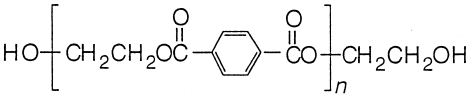

Experiment

Sample Preparation

10 mg/mL solutions of PET and the matrix, dithranol (1,8-di-hydroxy-9[10H]-anthracenone), were prepared using 1,1,1,3,3,3,-hexa-fluoro-iso-propanol as the solvent. A thin layer of the desired alkali halide (LiCl, NaI, or KI) was deposited on the sample target and 100 μL of a 1:5 mixture of PET and dithranol applied on top of the salt.

Ion Chromatography

A detailed description of the instrument used in this study has been previously published [29] so only an

overview will be given here. M^+PETn (M = Li, Na, K, and n = 2, 3, 4) ions are formed in a specially designed MALDI ion source [25], accelerated to 5 kV, and mass selected with a reverse geometry sector mass spectrometer. A 1–5 μs pulse of a mass selected oligomer is decelerated to 10–15 eV and injected into a variable temperature drift cell containing 2–3 torr of He gas. The temperature of the cell can be varied from 80 to 600 K. The ions are rapidly thermalized by collisions with He and drift through the cell under the influence of a weak electric field. Upon exiting the cell, the ions pass through a quadrupole mass filter and are detected by standard ion counting methods.

Data Analysis

The time it takes for the ions to drift through the cell is measured to yield an arrival time distribution (ATD). Ions with different drift times appear as different peaks in the ATD. This drift time is related to the mobility (K) of the ion by [30]

$$t_d = \frac{z}{KE} \quad (1)$$

where t_d is the drift time, z is the cell length, and E is the electric field strength. The mobility, in turn, is inversely proportional to the ion's collisional cross section through $\Omega^{(1,1)}$, the collision integral [30]

$$K = \frac{C}{\Omega^{(1,1)}} \quad (2)$$

where C is a constant that contains known information about the ion's charge and mass, the cell temperature, and the He pressure. The collision integral is extremely difficult to calculate for macromolecular systems but it has been shown that for large ions at temperatures $T \geq$ 300 K, $\Omega^{(1,1)}$ can be approximated by a modified hard sphere collision cross section (σ) [17, 24–26]. For temperatures <300 K a more detailed model of the ion–He interaction potential is required [31, 32]. In short, eqs 1 and 2 show that longer drift times correspond to lower mobilities and larger cross sections.

Theoretical Methods

AMBER 4.0 molecular mechanics/dynamics programs [33] were used to obtain further structural information from the mobility experiments. Because of the large number of facile bond rotations available to polymers, many different conformations, along with their corresponding local energy minima, are expected. Therefore, a series of annealings and energy minimizations are employed to allow a given structure to move across low energy barriers and undergo conformational changes. An initial structure is energy minimized, run through a 30 ps molecular dynamics simulation at 800 K, cooled to 0 K through another 10 ps molecular dynamics simulation, and energy minimized again. The final structure is then used as the starting point for another annealing/minimization run. This procedure was repeated until 100–150 low energy structures were obtained for each M^+PETn oligomer. The cross section of each structure was calculated using previously developed Monte Carlo techniques [17, 31] and compared to those obtained from the IC experiments. A scatter plot of cross section versus energy can then be constructed to help determine structural preferences.

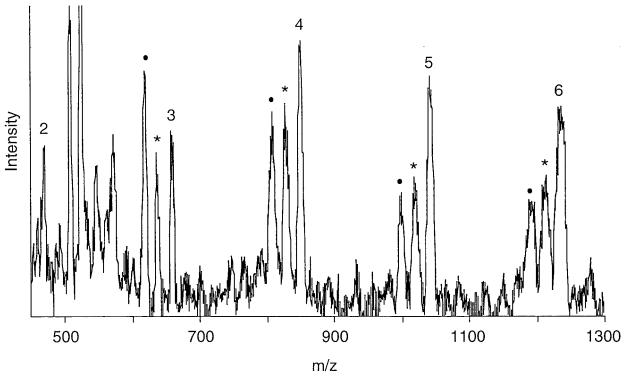

Figure 1. MALDI mass spectrum of PET cationized by Na^+. The peaks marked with an asterisk are the protonated PET series and the peaks marked with a filled circle are the Na^+ cationized series with H replacing CH_2CH_2OH as an end group. The large, unidentified peaks between n = 2 and n = 3 are due to the matrix.

Results

A typical mass spectrum is given in Figure 1. The sequence of Na^+PETn is indicated for n = 2 to 6. The two major peaks directly to lower mass of each Na^+PETn peak are the H^+PETn (asterisk) series (where H^+ replaces the Na^+ ion) and the $Na^+(PET)n$–H (filled circle) series (where –H replaces the $–CH_2CH_2OH$ as an end group). The unidentified intense peaks between n = 2 and n = 3 are matrix peaks. The ionization almost certainly continues above n = 6 but our sector mass spectrometer cannot go above m/z 1300.

The signal to noise ratio in the spectrum allows easy identification of the features mentioned above. However, these are marginal ion intensities for ion chromatography experiments where a single peak is mass selected, decelerated, and injected into the ion mobility cell, extracted from the cell, and an ATD measured. This process typically reduces the intensity of the beam by a factor greater than 10^3. As a consequence, we were not able to obtain reliable data for $n > 4$ because the larger species are more difficult to inject into the drift cell.

Typical ATDs for M = Li and K are given in Figure 2 for n = 2 to 4 at a cell temperature of 300 K. The ATDs for M = Na are very similar to those for M = K at this temperature. One striking feature is the fact that the Li^+PET3 ATD is bimodal, whereas the remaining five ATDs are single, symmetric, narrow peaks. This result

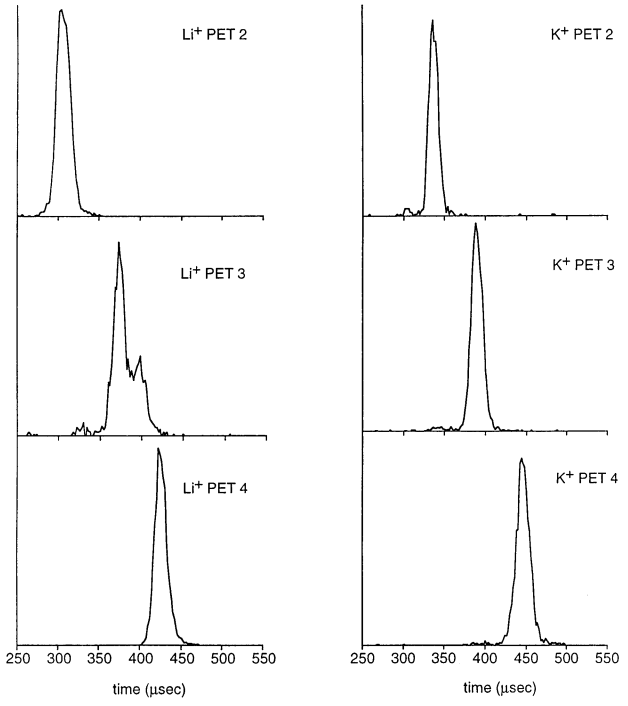

Figure 2. Arrival time distributions of Li^+PETn and K^+PETn for $n = 2$ to 4 at 300 K. As can be seen, the drift time increases with oligomer size. The two peaks observed for Li^+PET3 are due to two isomers with significantly different cross sections (see text).

is direct evidence for two isomers of Li^+PET3 with significantly different structures that do not interconvert on the experimental time scale at 300 K. The five remaining narrow peaks indicate either only a single isomer is present or isomer interconversion is rapid at 300 K.

Another feature evident in Figure 2 is that the average drift time for an oligomer increases with n. This is an expected result and indicates larger values of n lead to larger collision cross sections. For each system a series of ATDs was obtained for different drift voltages (i.e., drift times). From these data accurate values of the mobility could be measured (to a precision of $<1\%$ and an accuracy of $\sim 1\%$) and converted to cross sections using eq 2. These values are collected in Table 1.

In order to understand the structural correlations of these data, extensive molecular mechanics/dynamics calculations must be done. Using the annealing protocols discussed earlier, scatter plots of cross section versus energy were generated for 100 candidate structures. Examples are given in Figure 3 for the K^+PET2 and K^+PET3 systems. For K^+PET2 the 100 structures

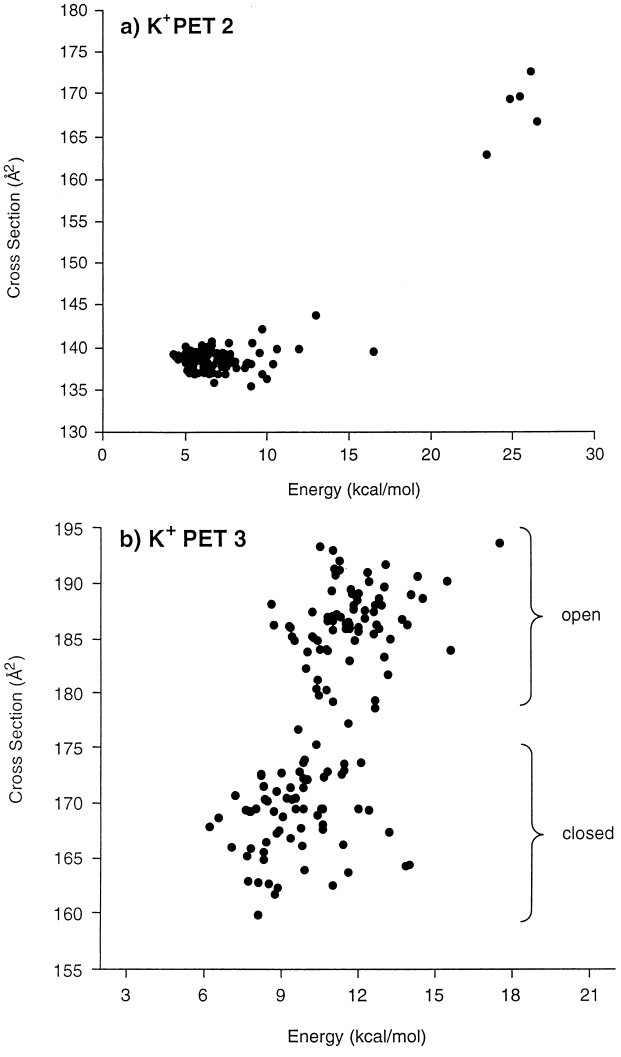

Figure 3. Cross section vs. energy scatter plot for (**a**) K^+PET2 and (**b**) K^+PET3. Each point represents one low energy structure calculated by the AMBER 4.0 suite of programs [33] using an annealing protocol described in the text. For K^+PET3, the cluster of points around 168 $Å^2$ correspond to the "closed" form and the group of points centered around 186 $Å^2$ correspond to the "open" form (see text).

Table 1. Experimental and theoretical cross sections of M^+PETn oligomers. All values are in $Å^2$ [a]

	$n = 2$		$n = 3$			$n = 4$	
				Theory			
M^+	Expt.	Theory	Expt.	Closed	Open	Expt.	Theory
Li	134	130	161, 183	161	178	192	194
Na	135	133	176	164	182	203	198
K	138	138	169	168	186	200	200

[a]Theory values from the AMBER 4.0 suite of programs [33]. See text.

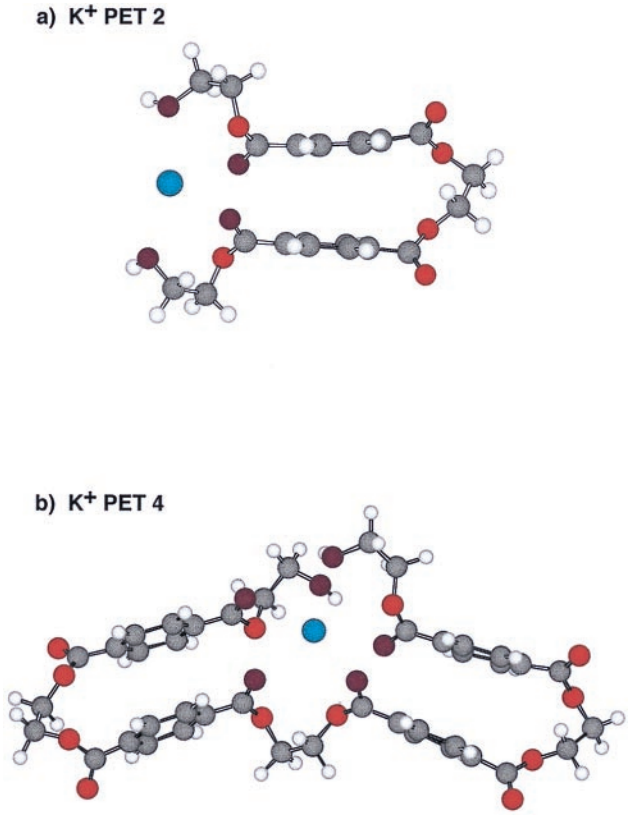

Figure 4. Typical low energy, compact structures found for (**a**) K^+PET2 and (**b**) K^+PET4. Carbon atoms are shown in gray, hydrogen atoms in white, oxygen atoms in red, and the K^+ ion in blue. Oxygen atoms coordinating to the K^+ ion are shown in purple. Similar structures were found for Li and Na.

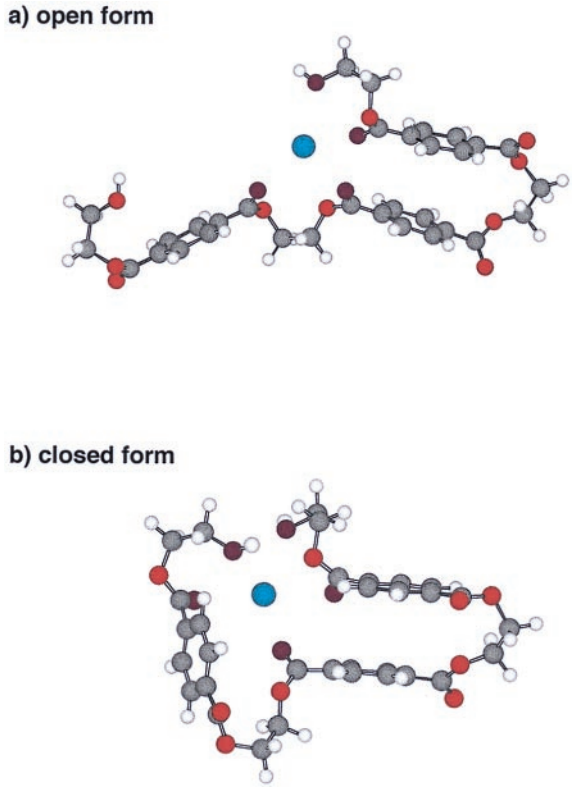

Figure 5. Typical low energy conformations found for the (**a**) open and (**b**) closed forms of K^+PET3. Similar structures were calculated for Li and Na.

are strongly clustered at low energy and at a cross section of 138 ± 2 Å^2. The compact structure that corresponds to these data is given in Figure 4a. A similar scatter plot is obtained for K^+PET*4* with the corresponding structure given in Figure 4b. Essentially identical structures were obtained for $n = 2$ and $n = 4$ for M = Li and Na as well.

A much different scatter plot is obtained for K^+PET*3*, shown in Figure 3b. Analysis of the various structures for the different cross section points indicates there are two basic isomers present: an open form, shown in Figure 5a, and a closed form, shown in Figure 5b. The closed form is responsible for the points clustered around the cross section 168 ± 3 Å$^+$ and the open form for the points around 186 ± 3 Å^2. The closed form is predicted to be more stable (by AMBER) by ~2 kcal/mol. Because the cross sections of the two forms differ by about 10%, they should have resulted in a bimodal ATD for K^+PET*3* unless they rapidly interconvert at 300 K. We will see this is the case when M^+PET*3* systems are considered in the Discussion.

Discussion

Although a number of the aspects of M^+PET*n* we are interested in overlap, they will be discussed separately so that we can emphasize the kind of information that can be extracted from studies of this type.

Oligomer Structures

One of the primary goals of the ion chromatography method is to obtain information on the macromolecular structure, especially in a solvent free environment. The key to successfully applying the method is to obtain accurate collision cross section data from ion mobility measurements and then to match these cross sections with those generated by the lowest energy structure(s) from the best available theoretical models. Because of the number of atoms in the macromolecule, classical molecular mechanics/dynamics methods are almost always required. We have found the AMBER 4.0 force field to provide excellent agreement with experiment for a variety of biological and synthetic polymers [18–20, 27, 28]. The same holds true for M^+PET2 and M^+PET*4* as shown in Table 1. In all six systems, agreement between experiment and theory is within 2% and for 4 of the 6 within 1%. Hence, the typical structures shown in Figure 4 for these systems are almost certainly correct.

There are two key structural elements in M^+PET2 and M^+PET*4*. First, in both structures "π stacking" of the benzene rings occurs. This is a robust structural feature in all oligomers, as we will see. The second

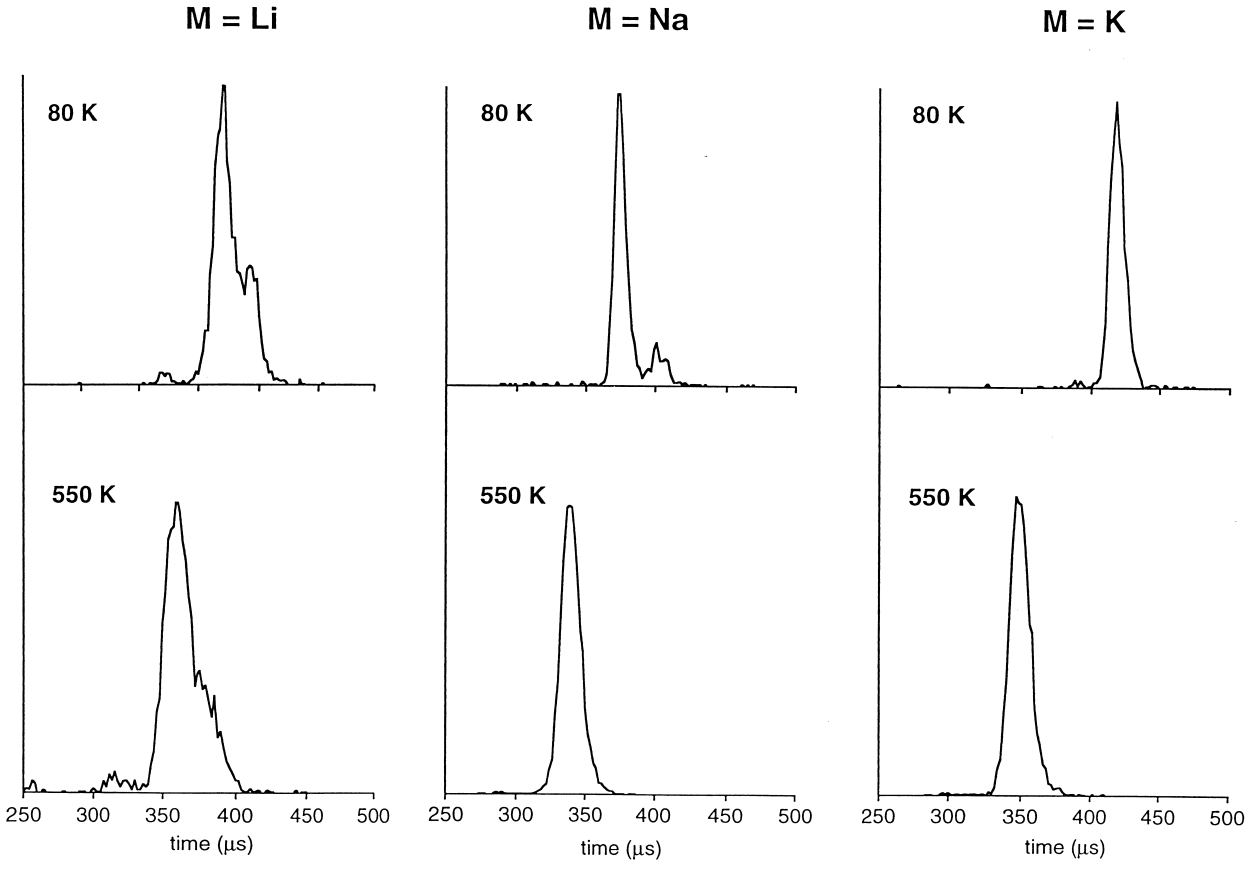

Figure 6. Arrival time distributions of M^+PET3 for M = Li, Na, and K at 80 and 550 K. The shorter time peak corresponds to the closed isomer and the longer time peak corresponds to the open isomer. For M = Li, both isomers are observed at each temperature in approximately the same ratio. For M = Na, the two isomers are separated at 80 K, whereas a mixture of the two are seen at temperatures >200 K. For M = K, only the closed form is observed.

important aspect is the coordination of the metal ion to either the terminal hydroxyl oxygens or the carbonyl oxygens. Typically four oxygens are coordinated but five coordination also occurs. It is, in fact, the M^+–oxygen coordination that drives the $n = 4$ structure to form two distinct π complexes rather than stacking the benzene rings one on top of the other—the favored structure for small neutral PET oligomers according to AMBER calculations.

The case for $n = 3$ is much more complex. As shown in the scatter plots, molecular mechanics predicts two structures. The first two monomer units π stack like the dimer and then the third either simply extends (open structure) or folds back to coordinate with the metal ion (closed structure). For all three metals the scatter plots predict the closed structure is somewhat more stable.

The experimental data for Li^+PET3 confirm the presence of both structures for this system with essentially quantitative agreement between experiment and theory (Table 1). The larger peak (at shorter times) for the closed structure is consistent with the AMBER prediction that this is the more stable structure. However, AMBER makes similar predictions about the closed and open forms of Na^+PET3 and K^+PET3 but only a single peak is observed in the ATDs for these systems. Furthermore, the experimental ATD for K^+PET3 gives a cross section in quantitative agreement with the closed form model cross section, whereas the experimental Na^+PET3 cross section falls between the model predictions for the open and closed forms. These issues will be dealt with in much more detail in the next section.

Folding Energetics in M^+PET3

In order to test for rapid isomerization, it is useful to change the temperature of the mobility cell. In Figure 6 are ATDs for all three M^+PET3 systems at 80 and 550 K. There are two important results apparent in the data. First, the bimodal character of the Li^+PET3 system is retained at both temperatures as is the relative intensities of the two peaks. Consequently, the isomerization barrier in this system is quite high. We will come back to this point shortly.

The second feature that is apparent is the 80 K Na^+PET3 ATD is now bimodal with a larger peak at

shorter times (closed form) and a smaller peak at longer times (open form). By varying T between 80 and 180 K a series of ATDs of varying shape were observed. By adapting kinetic theory of ions drifting in gases [34] to our conditions, isomerization rate constants could be extracted as a function of temperature. A plot of ln k versus $1/T$ yielded an isomerization barrier of 1.6 kcal/mol going from the open to closed form in Na^+PET3. By fitting the 80 K relative intensities using an RRKM model, we determined the closed form is more stable than the open form by ~0.5 kcal/mol in good agreement with molecular mechanics estimates. The details of the experiments and analysis for Na^+PET3 have been communicated elsewhere [35].

The K^+PET3 ATDs show no bimodal character even at 80 K in spite of the fact the scatter plot indicates both open and closed forms are minima on the potential energy surface. From these data we can infer the barrier to isomerization is less than 1 kcal/mol. (As we shall see in a later section, if the barrier between the two forms was substantial, the open form should have been observed.) Also, because the experimental cross section data are in perfect agreement with the model cross sections for the closed form (Table 1), the inference is the closed form is considerably more stable then that of the open form. Molecular mechanics predicts, in fact, the closed form is ~2 kcal/mol more stable than the open form.

The Li^+PET3 system retains the same fractions of open to closed forms from 80 to 550 K indicating a high isomerization barrier. Hence, we can unambiguously conclude this barrier is a strong function of alkali ion, with a low barrier for K^+, intermediate for Na^+, and high for Li^+. An estimate of the barrier height in Li^+PET3 can be obtained by using a model originally developed for carbon cluster isomerization barriers [36]. The equilibrium constant at the energy of the barrier height between the two forms is given by

$$K(E) = \frac{[\text{open}]_E}{[\text{closed}]_E} = \frac{\rho_o(E - \Delta E)}{\rho_c(E)} \quad (3)$$

where the energy E is measured from the bottom of the closed form to the isomerization barrier height, ΔE is the energy difference between the open and closed forms, and ρ_o and ρ_c are the densities of states for the open and closed forms, respectively, at the energies indicated. The model assumes that the system is initially formed at an energy larger than E and that subsequent collisions with the bath gas quickly cool the system. A schematic figure that exemplifies the process and defines the various energies is given in Figure 7. Once the system reaches energy E (i.e., the barrier height) isomerization ceases and further cooling freezes the distribution at this energy. Hence the measured peak heights of the open and closed forms are thus assumed to be proportional to the isomer populations at energy E. As a result, an experimental value of $K(E)$ can

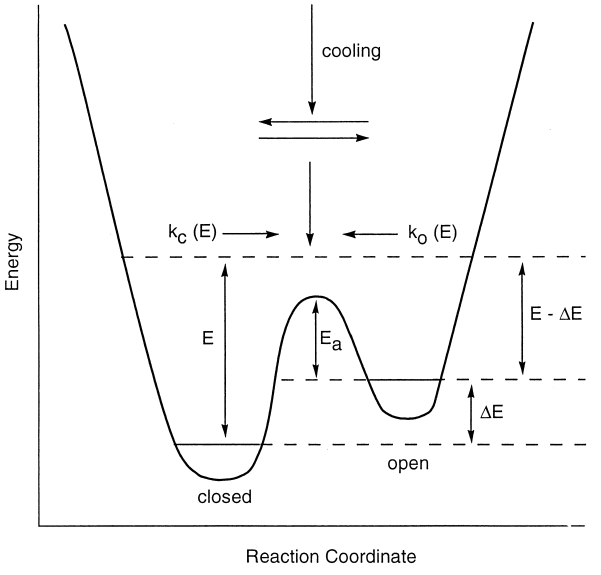

Figure 7. A reaction coordinate diagram for the isomerization of open and closed forms of M^+PET3. Definitions of the labels in the diagram are given in the text.

be established. For Na^+PET3 we were able to measure the barrier height experimentally and so calculations of the densities of states required to reproduce $K(E)$ directly yielded ΔE. However, in Li^+PET3 both E and ΔE are unknown. Molecular dynamics can be used to estimate ΔE from the scatter plot, yielding $\Delta E = 5 \pm 1$ kcal/mol. We can then calculate $K(E)$ for a range of E with the results given in Figure 8.

In this figure the horizontal dashed lines give the uncertainty in the measured value of $K(E) = 0.26 \pm$

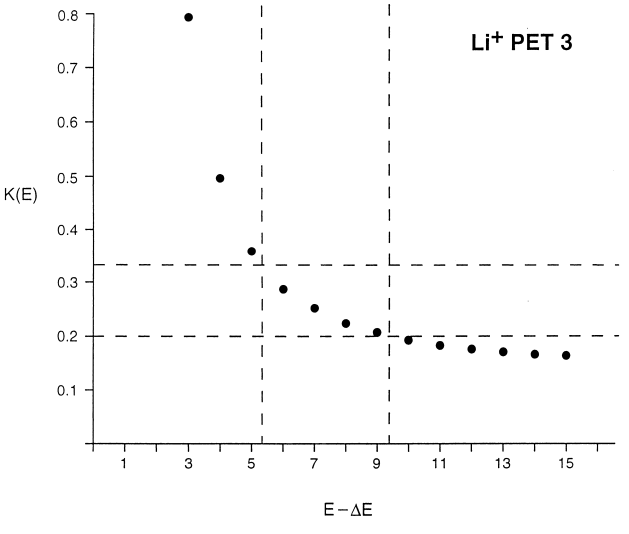

Figure 8. A plot of $K(E)$ vs. $E - \Delta E$ as defined in eq 3 (solid points). The two horizontal dashed lines represent the upper and lower limits of $K(E)$ as determined by the intensities of the ATD peaks. The two vertical dashed lines represent the resulting estimates of the barrier height for the open to closed isomerization for Li^+PET3.

Table 2. Energetics of the M^+PET3 systems. All values in kcal/mol

M	$E^{\ddagger}_{O\rightarrow C}$[a]	$E^{\ddagger}_{C\rightarrow O}$[b]	ΔE[c]
Li	7 ± 2[d]	12 ± 3	5 ± 2
Na	1.6	2.1	0.5
K	1.0	3 ± 1	2 ± 1

[a]The barrier for isomerization from the open to closed form.
[b]The barrier for isomerization from the closed to open form.
[c]$\Delta E = E_{open} - E_{closed}$. The Na number is experimental [35] and the Li, K numbers come from molecular dynamics calculations using the AMBER 4.0 suite of programs [33].
[d]Rigorously, this is only a lower limit (see text).

0.06. The solid points give the calculated values of $K(E)$. The vertical dashed lines yield 7 ± 2 kcal/mol for the open → closed isomerization barrier in Li^+PET3. The value of the barriers, and ΔE values, for the three M^+PET3 systems are collected in Table 2.

The value of $K(E)$ for Li^+PET3 was taken at the highest laser powers used for these MALDI experiments in order to maximize the internal energy in the oligomer. The model used to determine the isomerization barrier assumes all desorbed oligomers initially have energies above the isomerization barrier. This probably is not the case, as will be shown in the next section, and so the barrier reported in Table 2 for this system should be treated as a lower limit.

Several interesting trends are present in the data of Table 2. First, the isomerization barriers are fairly strong functions of the metal ion, decreasing as the metal gets larger. This is almost certainly due to the weakening of the M^+–O interaction energies as metal size increases. As shown in a later section, this variation in interaction energy with metal size will also affect the mass spectra observed as the metal ion is varied.

The second effect apparent in the data exemplifies the subtle nature of the interactions that determine conformational stability. For all three metals, the closed form is more stable than the open form. However, the magnitude of ΔE depends on metal ion in a nonmonotonic way. Although the difference is clearly greatest for Li^+, the K^+ ion has the second largest value of ΔE with Na^+ last. There are two balancing energetic terms that generate this effect. There is strain energy associated with the folding required to form the closed isomer, but there is also the energy payback received by increased interaction with the metal center and oxygen atoms. For M = Li, the interaction of the metal ion with the oxygen centers easily overcomes the strain energy, even though the degree of folding is maximized in this system. Thus, the closed form is strongly energetically favored. For M = Na, the two effects nearly balance. The strain energy is not as high as in Li (due to the larger Na ion) but the Na^+–O interaction energy is also not as high as Li. However, the decrease in strain energy apparently counteracts the decrease in Na^+–O interaction energy resulting in similar energies for the sodiated open and closed forms (and a small ΔE value). Finally, for the significantly larger K^+ system, the decrease in strain energy (relative to Na^+) overcomes the loss of K^+–O interaction energy leading to an increase in ΔE.

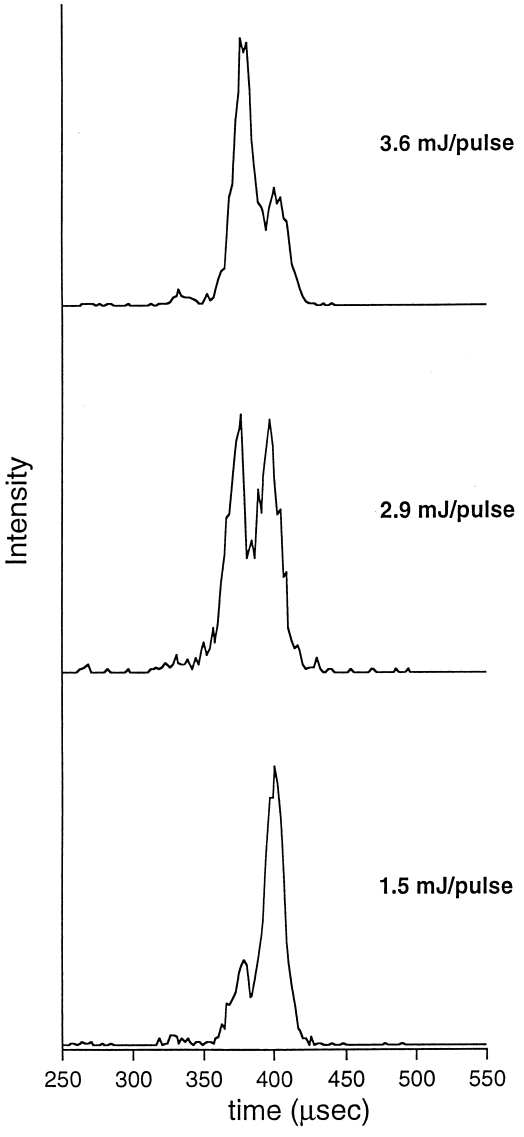

Figure 9. 300 K ATDs for Li^+PET3 as a function of laser power. (See Scheme **1** and text.)

The MALDI Mechanism

One of the ongoing areas of interest to practitioners of MALDI is the mechanism by which ionization occurs. There are two broad possibilities, each of which has interesting further dimensions:

(1) Ejection of preformed ions from the analyte/matrix composite.
(2) Ejection of neutral analyte followed by ionization in the gas phase.

Some interesting and unusual behavior for the Li^+PET3 system allow for a degree of insight into the process rarely found experimentally.

When trying to understand the insensitivity of the bimodal Li^+PET3 ATD to temperature, and to establish quantitatively the isomerization barrier, we decided to vary the power level of the laser used in the MALDI source. The 300 K ATDs for three different power levels are given in Figure 9. The top panel represents our usual operating conditions and reproduces the 300 K data in Figure 2. In this instance the ratio [open] : [closed] is ~0.26 (as indicated in Figure 7). However, as the laser power is reduced to 2.9 mJ/pulse from 3.6 mJ/pulse, the [open] : [closed] ratio becomes ~1.0 and as the laser power is further reduced to 1.5 mJ/pulse the [open] : [closed] ratio increases to ~6.0. Hence, by simply decreasing the laser power, the fractional abundance of the less stable open isomer is enhanced by about a factor of 25! Because everything happening after the laser desorption in the MALDI source is identical for the three experiments, the differences in the ATDs must be due to the formation mechanism of the ions.

At first glance, the results in Figure 9 are counterintuitive because decreasing the laser power decreases the average energy available to the system, yet dramatically increases the fraction of the higher energy isomer. These data appear to rule out desorption of preformed ions because the possibility of formation of preformed ions in the matrix must be independent of the laser power, and any increase in energy of this initial distribution would favor isomerization to the more stable closed form. For example, if ions are preformed in the matrix, it is reasonable to assume that the more stable closed form would dominate (or at least be competitive with) the less stable open form. Hence, as laser power is reduced, the closed form should either increase its fractional abundance or hold its own. However, the experiment clearly indicates the closed form essentially disappears at lowest laser powers, strongly suggesting preformed ions are not significantly contributing to the MALDI signal. Consequently, the ionization must take place following laser impact and thus almost certainly occur in the ascending plume in the gas phase.

A mechanism consistent with the results is given in Scheme 1. Molecular dynamics calculations indicate the lowest energy form of neutral PET3 is s-shaped with the three benzene rings stacking on top of each other. This is the intuitive structure because π stacking is worth about 10 kcal/mol and there is no metal ion stabilizing the system. Hence, it is reasonable to assume such structures dominate in the solid phase. Once ejected into the gas phase, the s-shaped structure should again dominate. At lower laser powers it is possible the fraction of s-shaped structures desorbed approaches 1.0 (i.e., $f \sim 1.0$ in Scheme 1). As laser power increases, vibrational energy increases in PET3 and opening of the s-shaped structure will occur because entropy (or more correctly the density of states) favors the open structure at higher internal energies.

When the s-shaped structure encounters the metal ion, dynamics will require it to initially form the open

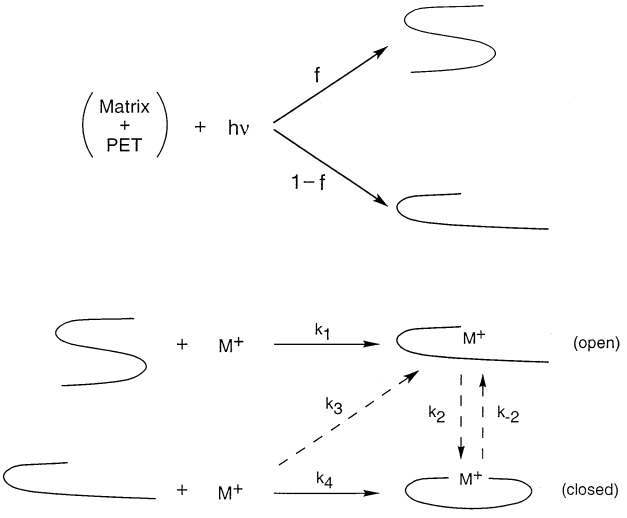

Scheme 1

M^+PET3 structure, as indicated by k_1 in Scheme 1. A fraction of these open structures may have sufficient energy to isomerize to the closed structure as indicated by k_2. If, on the other hand, an open PET3 neutral encounters a metal ion it can initially form either the open or closed forms of M^+PET3.

Now consider the effect of internal energy on these processes. At lowest internal energies where $f \sim 1.0$, only open M^+PET3 ions are formed as the initial association product. This species will be rapidly collisionally stabilized in the plume. If the isomerization barrier is high, $k_2 \sim 0$ and only open M^+PET3 will be formed. This scenario would explain the fact that Li^+PET3 is almost exclusively in the open form at lower laser powers because the isomerization barrier is relatively high (7 ± 2 kcal/mol). On the other hand, 300 K ATDs for Na^+PET3 and K^+PET3 are independent of laser power. In these cases the isomerization barrier is too low to prevent rapid isomerization in the 300 K bath gas and any preferential formation of the open form in the MALDI process cannot be observed. In terms of Scheme **1**, $k_2 > k_{-2}$ for Na^+PET3 and $k_2 \gg k_{-2}$ for K^+PET3.

As the laser power increases, two factors affect the observed isomer distribution in Li^+PET3. First, the s-shaped PET3 neutral can isomerize to the open form before encountering a Li^+ ion and second, the open form Li^+PET3 ions can isomerize to the closed form (i.e., k_2 increases with internal energy). Both effects increase the fraction of closed form eventually observed in the experiment. At highest laser powers it is expected that the Li^+PET3 system is energetically well above the isomerization barrier before injection into the mobility cell. This expectation was used as an assumption in deriving the isomerization barrier of 7 ± 2 kcal/mol in the previous section. If there is still some preferential formation of open Li^+PET3 at highest laser powers, then the barrier is a lower limit, as previously mentioned.

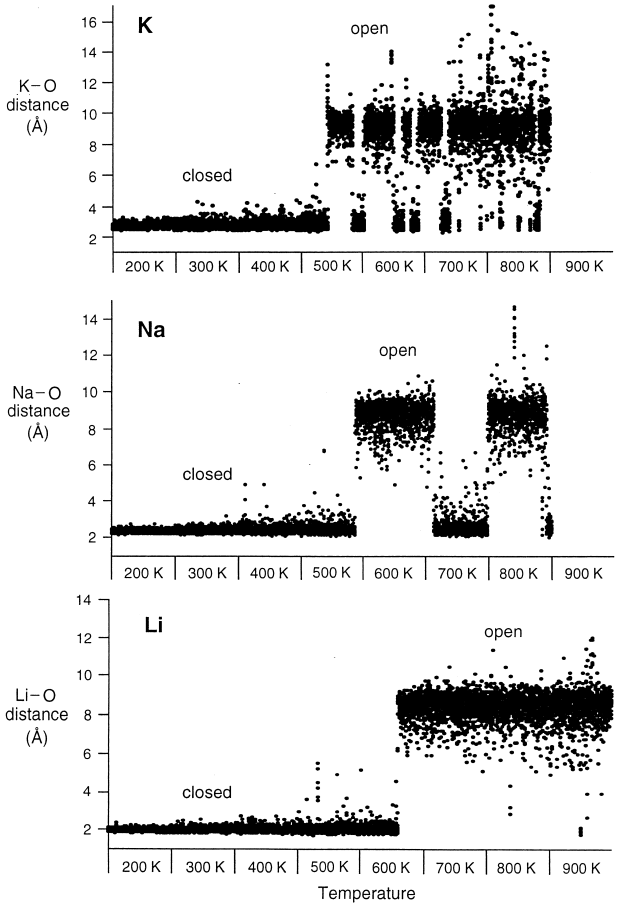

Figure 10. A plot of the distance between M^+ and a selected carbonyl oxygen atom on PET3 as a function of time and temperature for M = Li, Na, and K. M^+–O distances of ~2 Å correspond to the closed form, whereas M^+–O distances >7 Å correspond to the open isomer. The temperature is held constant at 200 K between the first two tic marks, 300 K between the next two tic marks, etc.

Isomerization Dynamics

To get a better feel for the isomerization process, it is useful to investigate the dynamics. Consequently, we followed the dynamics by plotting the distance between the terminal carbonyl oxygen and the metal ion as a function of time and temperature for M = Li, Na, and K. In each case the system was started in the more stable closed form at 200 K. The structures were sampled and cross sections calculated every 0.5 ps and each temperature run for 1000 ps, or 2000 structures in all. The temperature was then raised by 100 K increments to 800 K (Na and K) and 900 K (Li) and the M^+–O distance for the terminal carbonyl oxygen was monitored. Results are given in Figure 10.

A number of features are evident. First at 200 K, the average M^+–O distance varies from 2.0 ± 0.2 $Å^2$ for Li^+ to 2.8 ± 0.3 $Å^2$ for K^+ with Na^+ in between. These distances directly correlate with the strength of the electrostatic bonds between the metal centers and oxygen atoms with Li^+ having the strongest and K^+ the weakest bonds.

Second, through 400 K no isomerization occurs in any system. This result does not correlate with experiment for either Na^+ or K^+ where in the former case isomerization was experimentally observed down to 80 K. The reason for the discrepancy is almost certainly one of time scale. In the experiment, the ATDs occurred over hundreds of microseconds, or 10^5 to 10^6 larger times than the simulations. It is common in molecular dynamics simulations that realistic time scales cannot be sampled. The solution often prescribed is to raise the temperature to accelerate the process as we have done here.

K^+PET3 is the first to isomerize about 400 ps through the 500 K dynamics run. The system then undergoes increasingly frequent isomerizations as the temperature increases, at first maintaining an "open" or "closed" conformation for several hundred picoseconds but eventually the motion becomes almost chaotic with "totally open" conformations occurring about as frequently as the "closed" conformation. It is also apparent that the open conformations undergo larger structural excursions than the closed, a common feature for all three metal ions.

The Na^+PET3 system is the next to isomerize after ~900 ps at 500 K. In this case, isomerization occurs much less frequently than in K^+PET3 with a particular conformation surviving about 1000 ps before isomerizing. The rate of isomerization is directly related to the barrier height with the larger Na^+PET3 barrier slowing down the process.

Finally, in Li^+PET3 the closed form opens up after ~600 ps at 600 K and then remains in the open conformation(s) through 900 K (with one brief exception). Hence, the system with the highest barrier opens up at the highest temperature and undergoes the least isomerization over the ranges of time and temperature sampled.

The general trends observed in the dynamics are in excellent agreement with the experimentally determined barriers to isomerization. This fact generates confidence in the AMBER 4.0 parametrization used in the calculations. Having two experimental observables (energetics and cross sections) agree with theory gives strong evidence that the calculated structures shown here are good representations of the actual M^+PET*n* oligomer structures.

Mass Spectra

One of the principal reasons for our initial involvement with the PET system was the observation that the apparent oligomer distribution as measured by MALDI-TOF is a reasonably strong function of the cationizing metal ion [15]. Although a detailed, quantitative understanding of this effect is still being developed and will be published elsewhere, it is useful to point out the main qualitative reasons for it here.

Table 3. Binding energies in kcal/mol of PET*n* oligomers to various alkali ions[a,b]

Alkali ion	1	3	5	7
Li	44	79	88	111
Na	34	54	66	88
K	26	41	54	69
Cs	21	32	41	57

[a]From AMBER 4.0 suite of programs [33].
[b]Should be considered as relative values only. Uncertainties of ±5% expected due to large isomer distribution, especially for larger values of *n*.

The principal observation was the oligomer distribution for a specific PET sample appeared to be centered at $n = 4$ to 6 when cationized by Li^+ and increased to $n = 12$, 13 when cationized by Cs^+ with the remaining alkali metal ions somewhere in between. Little or no skeletal fragmentation was observed in all systems, indicating this was not the source of the spectral shifts.

The key to understanding these data lies in the relative binding energies of the metal ions to the oligomers and how this energy depends on oligomer size. The experiment measures ions that actually make it from the MALDI source to the detector. Under typical source conditions, the oligomers are generated internally excited by the laser desorption event and are possibly further excited by collisions in the acceleration field following the source. Although backbone fragmentation can be one outcome of this internal excitation, loss of metal ion will predominate, particularly for the more weakly bound metal ions [27, 37].

Some results of AMBER 4.0 calculations on metal ion binding energies to oligomers with $n = 1$, 3, 5, and 7 are given in Table 3. Two factors stand out. First, the metal ion binding energies increase with oligomer size and second, these binding energies increase as the metal ion becomes smaller. The Li^+ ion is bound to the monomer by essentially the same amount of energy as the Cs^+ ion is to the heptamer. In contrast, the Cs^+ ion is bound to the monomer 5 times less strongly than the Li^+ ion is bound to the heptamer.

These relative binding energies are reflected in the structures of the ions as shown in Figure 11 for the M^+PET7 system. The Li^+ ion is buried inside the heptamer, the K^+ ion, being larger, is partially exposed, and the Cs^+ ion, being even larger, essentially sits on the surface. Hence, in addition to the actual binding energies of the various metal ions to the oligomers, there may be barriers involved along the dissociation reaction coordinate for the smaller ions associated with oligomer reorganization. In order to fully understand these systems, the dissociation mechanism will have to be studied in detail.

It is not unreasonable to assume that the PET oligomers cationized by Li^+ have about the same internal energy as those cationized by Cs^+ because collisional excitation/cooling is expected to dominate the energy distribution in a given species (although the former may be slightly more internally excited due to their higher metal ion attachment energies). RRKM theory indicates that the unimolecular rate constant for metal ion loss will be a strong function of the internal energy above the dissociation threshold. As a consequence, for systems with nearly the same internal energy but strongly different dissociation thresholds the lifetimes of the ions will be greatly different. Looked at another way, in order to meet a certain minimal lifetime for detection, a weakly bound M^+–PET*n* system will have to have a much higher density of states (i.e., have a larger value of *n*) than a more strongly bound system. Because the experiment sets a fixed time window, an oligomer with a fixed value of *n* is more likely to reach the detector if it is cationized by Li^+ than if it is cationized by Cs^+. In order to obtain the same lifetime, the Cs^+ ion would have to be attached to an oligomer with a larger value of *n*. Although working out all the details is a formidable task for systems this size, good progress is being made. For the present, however, it is best to simply assume that Li^+ or Na^+ cationization will give more reliable oligomer distributions than larger alkali ions. Finally, this interpretation is consistent with CID experiments on PMMA [27, 37].

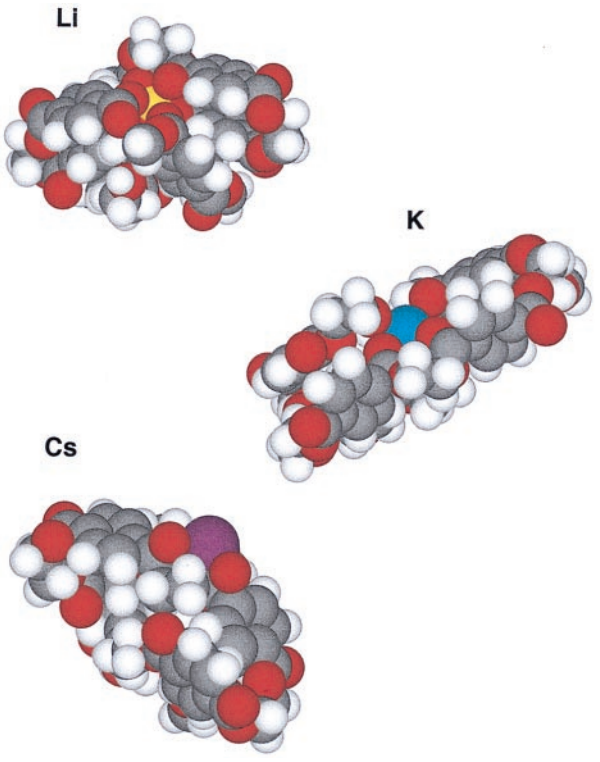

Figure 11. Space filling models of the lowest energy structures found for Li^+PET7, K^+PET7, and Cs^+PET7. The Li^+ ion is yellow, the K^+ ion is blue, and the Cs^+ ion is purple. The small Li^+ ion is embedded in the PET oligomer, whereas the larger Cs^+ ion is very much exposed and basically rests on the outside surface of the oligomer.

Conclusions

The M^+–PETn family of oligomers provides a rich system for studying a number of fundamental and practical aspects of macromolecular behavior. Specifically, we are able to conclude from this study:

For $n = 2$ and 4, the PET oligomers π stack with the metal ion coordinating to both the terminal hydroxyl oxygens and several carbonyl oxygens.

For $n = 3$, there are two competing isomers: an "open" form where the third PET moiety attaches to the dimer structure and extends into space and a "closed" form that is slightly more stable where the third monomer bends back around so the terminal hydroxyl oxygen can interact with the metal ion.

For Na^+PET3, the open and closed isomeric forms are in equilibrium and their relative populations obtainable using the ion chromatography method from 100 to 180 K. An Arrhenius analysis led to an open to closed isomerization barrier of 1.6 kcal/mol.

For Li^+PET3, both the open and closed isomers are observed with unchanging relative populations from 80 to 550 K. By using an RRKM based analysis developed for isomerization barrier determination in carbon clusters, it was possible to extract an open to closed isomerization barrier of 7 ± 2 kcal/mol.

The fractional populations of the open and closed isomers of Li^+PET3 were observed to be strong functions of the laser power in the MALDI source. The lower the laser power, the greater the population of the less stable open form isomer. A mechanism was proposed that explained this seemingly nonintuitive result that involved gas phase cationization of the energetically favored s-shaped, π-stacked, neutral PET3 oligomer.

Molecular dynamics simulations were done over the temperature range of 200 to 800 K for Li^+, Na^+, and K^+ bound to PET3. The observed dynamics were entirely consistent with the experimentally observed fact of the isomerization barriers increasing from K^+ to Na^+ to Li^+. Because both experimental cross sections and barrier determinations agree with theory, extra confidence can be given to the structures of the various Na^+PET3 systems generated by the AMBER 4.0 force field.

The mass spectrum of a single PET sample gives oligomer distributions that are a function of the metal ion. This phenomenon is qualitatively explained in terms of relative binding energies of the various alkali ions to the oligomer and in terms of the M^+PETn structures involved.

Acknowledgments

The authors gratefully acknowledge the support of the Air Force Office of Scientific Research under grants F49620-96-1-0033 and F49620-96-1-0257 and for partial support of the National Science Foundation under grant CHE-9729146. MTB would also like to convey his pleasure and heartfelt thanks that ASMS chose to award the 1998 Biemann Medal to Bob Squires and his profound sense of loss at the passing of one of his most respected colleagues and cherished friends.

References

1. Davidson, J. N. *Biochemistry of Nucleic Acids*; Academic: New York, 1997.
2. *Macrocyclic Compounds in Analytical Chemistry*; Zolotov, Y. A., Ed.; Wiley–Interscience: New York, 1997.
3. Creighton, T. E., *Proteins: Structures and Molecular Properties*, 2nd ed.; Freeman; New York, 1993.
4. *Encyclopedia of Polymer Science and Engineering*, 2nd ed. Mark, H. F.; Bikales, N. M.; Overberger, C. G.; Menges, G.; Kroschwitz, J., Eds.; Wiley–Interscience: New York, 1985.
5. Hillenkamp, F.; Karas, M.; Beavis, R. C.; Chait, B. C. *Anal. Chem.* **1991,** *63*, 1193A.
6. Bahr, U.; Deppe, A.; Karas, M.; Hillenkamp, F. *Anal. Chem.* **1992,** *64*, 2866.
7. Montaudo, G.; Montaudo, M. S.; Puglisi, C.; Samperi, F. *Rapid Commun. Mass Spectrom.* **1995,** *9*, 453, and references therein.
8. Williams, J. B.; Gusev, A. I.; Hercules, D. M. *Macromolecules* **1997,** *30*, 3781.
9. Pastor, S. J.; Wilkins, C. L. *J. Am. Soc. Mass Spectrom.* **1997,** *8*, 225.
10. Montaudo, G.; Montaudo, M. S.; Puglisi, C.; Samperi, F. *J. Polym. Sci. Part A: Polym. Chem.* **1996,** *34*, 439.
11. De Koster, C. G.; Duursma, M. C.; van Rooij, G. J.; Heeren, R. M. A.; Boon, J. J. *Rapid Commun. Mass Spectrom.* **1997,** *11*, 520.
12. Jackson, A. T.; Yates, H. T.; Lindsay, C. I.; Didier, Y.; Segal, J. A.; Scrivens, J. H.; Critchley, G.; Brown, J.; Green, M. R.; Bateman, R. H. *Rapid Commun. Mass Spectrom.* **1997,** *11*, 520.
13. Lehman, E.; Knochenmuss, R.; Zenobi, R. *Rapid Commun. Mass Spectrom.* **1997,** *11*, 1483.
14. Dogruel, D.; Nelson, R. W.; Williams, P. *Rapid Commun. Mass Spectrom.* **1996,** *10*, 801.
15. Jackson, A. T.; Yates, H. T.; MacDonald, W. A.; Scrivens, J. H.; Critchley, G.; Brown, J.; Deery, M. J.; Jennings, K. R.; Brookes, C. *J. Am. Soc. Mass Spectrom.* **1997,** *8*, 132. Deery, M. J.; Jennings, K. R.; Jasieczek, C. B.; Haddleton, D. M.; Jackson, A. T.; Yates, H. T.; Scrivens, J. H. *Rapid Commun. Mass Spectrom.* **1997,** *11*, 57.
16. Kemper, P. R.; Bowers, M. T. *J. Phys. Chem.* **1991,** *95*, 5134; Bowers, M. T.; Kemper, P. R.; von Helden, G.; van Koppen, P. A. M. *Science* **1993,** *260*, 1446.
17. von Helden, G.; Hsu, M.-T.; Kemper, P. R.; Bowers, M. T. *J. Chem. Phys.* **1991,** *95*, 3835. von Helden, G.; Kemper, P. R.; Gotts, N. G.; Bowers, M. T. *Science* **1993,** *259*, 1300. von Helden, G.; Hsu, M.-T.; Gotts, N. G.; Bowers, M. T. *J. Phys. Chem.* **1993,** *97*, 8182. Gotts, N. G.; von Helden, G.; Bowers, M. T. *Int. J. Mass Spectrom. Ion Process* **1995,** *149/150*, 217.
18. Wyttenbach, T.; von Helden, G.; Bowers, M. T. *J. Am. Chem. Soc.* **1996,** *118*, 8355.
19. Lee, S.; Wyttenbach, T.; Bowers, M. T. *Int. J. Mass Spectrom. Ion Processes* **1997,** *167/168*, 605.
20. Wyttenbach, T.; Bushnell, J. E.; Bowers, M. T. *J. Am. Chem. Soc.* **1998,** *120*, 5098.
21. Clemmer, D. E.; Hudgins, R. R.; Jarrold, M. F. *J. Am. Chem. Soc.* **1995,** *117*, 10141.
22. Shelimov, K.; Jarrold, M. F. *J. Am. Chem. Soc.* **1996,** *118*, 10313.
23. Clemmer, D. E.; Jarrold, M. F. *J. Mass Spectrom.* **1997,** *32*, 577.
24. von Helden, G.; Wyttenbach, T.; Bowers, M. T. *Science* **1995,** *267*, 1483.
25. von Helden, G.; Wyttenbach, T.; Bowers, M. T. *Int. J. Mass Spectrom. Ion Processes* **1995,** *146/147*, 349.
26. Wyttenbach, T.; von Helden, G.; Bowers, M. T. *Int. J. Mass Spectrom. Ion Processes* **1997,** *165/166*, 377.
27. Gidden, J.; Jackson, A. T.; Scrivens, J. H.; Bowers, M. T. *Int. J. Mass Spectrom.* **1999,** *188*, 121.

28. Gidden, J.; Jackson, A. T.; Scrivens, J. H.; Bowers, M. T., to be published.
29. Kemper, P. R.; Bowers, M. T. *J. Am. Soc. Mass Spectrom.* **1990,** *1*, 197.
30. Mason, E. A.; McDaniel, E. W. *Transport Properties of Ions in Gases*; Wiley; New York, 1988.
31. Wyttenbach, T.; von Helden, G.; Batka, J. J.; Carlat, D.; Bowers, M. T. *J. Am. Soc. Mass Spectrom.* **1997,** *8*, 275.
32. Mesleh, M. F.; Hunter, J. M.; Schvartsburg, A. A.; Schatz, G. C.; Jarrold, M. F. *J. Phys. Chem.* **1996,** *100*, 16082. Schvartsburg, A. A.; Schatz, G. C.; Jarrold, M. F., *J. Chem. Phys.* **1998,** *108*, 2416.
33. Pearlman, D. A.; Case, D. A.; Caldwell, J.; Seibel, G. L.; Singh, U. C.; Weiner, P.; Kollman, P. A. AMBER 4.0, UCSF, CA, 1991.
34. Gatland, I. R. *Case Studies At. Phys.* **1974,** *4*, 369.
35. Gidden, J.; Wyttenbach, T.; Batka, J. J.; Weis, P.; Jackson, A. T.; Scrivens, J. H.; Bowers, M. T. *J. Am. Chem. Soc.* **1999,** *121*, 1421.
36. von Helden, G.; Gotts, N. G.; Bowers, M. T. *Chem. Phys. Lett.* **1993,** *212*, 241; von Helden, G.; Gotts, N. G., Palke, W. E.; Bowers, M. T. *Int. J. Mass Spectrom. Ion Processes* **1994,** *138*, 33.
37. Scrivens, J. H.; Jackson, A. T.; Yates, H. T.; Green, M. R.; Critchley, G.; Brown, J.; Bateman, R. H.; Bowers, M. T.; Gidden, J. *Int. J. Mass Spectrom. Ion Processes* **1997,** *165/166*, 363.